Elastic phase response of silica nanoparticles buried in soft matter

Laurene Tetard,[1,2] Ali Passian,[1,2,a)] Rachel M. Lynch,[1] Brynn H. Voy,[1] Gajendra Shekhawat,[3] Vinayak Dravid,[3] and Thomas Thundat[1,2]
[1]*Biosciences Division, Oak Ridge National Laboratory, Oak Ridge, Tennessee 37831, USA*
[2]*Department of Physics, University of Tennessee, Knoxville, Tennessee 37996-1200, USA*
[3]*Materials Science and Engineering Department, Northwestern University, Evanston, Illinois 60208, USA*

(Received 14 July 2008; accepted 29 August 2008; published online 2 October 2008)

Tracking the uptake of nanomaterials by living cells is an important component in assessing both potential toxicity and in designing future materials for use *in vivo*. We show that the difference in the local elasticity at the site of silica (SiO_2) nanoparticles confined within a macrophage enables functional ultrasonic interactions. By elastically exciting the cell, a phase perturbation caused by the buried SiO_2 nanoparticles was detected and used to map the subsurface populations of nanoparticles. Localization and mapping of stiff chemically synthesized silica nanoparticles within the cellular structures of a macrophage are important in basic as well as applied studies. © *2008 American Institute of Physics*. [DOI: 10.1063/1.2987460]

Analogous to macroscale ultrasonic applications, such as imaging a fetus in a womb, in the realm of the nanoscale, one may elastically perturb the interior of a cell or a vesicle to determine whether or not nanoparticles may reside inside. The extent to which nanostructures, as opposed to their bulk counterparts, retain their extensive material properties is clearly of importance for such perturbation. In this letter, we capitalize on the stiffness and density of silica to visualize nanoparticles within the interior of a mouse macrophage by employing the scattering of ultrasonic waves. While of tremendous importance as a carrier in drug delivery, certain types of silica are known as toxic particles and are often used as a positive control in toxicology studies because of the inflammatory response they can provoke. In such cases, silica is a well-characterized pulmonary pathogen, and low doses of nanosized SiO_2 particles have been shown to induce lung inflammation and tissue damage. While the focus of the current letter is not the mechanism of cellular entry and the controversies surrounding this central topic,[1] we note that nanoparticle morphology, size dependence, and amphipathic properties have been implicated to play a role in the uptake process.[1,2] Therefore, cell-type specific, as well as nanoparticle specific, nanoscale observation of localized events is of current importance rendering the presented results here of direct relevance.

Utilizing a recent innovation in force microscopy,[3] nanoparticles that had initially been introduced *in vivo* via the process of aspiration [see Fig. 2(a)] were localized within the cellular structures of broncheoalveolar macrophages. Silicon dioxide (SiO_2), a common constituent of sand, may form nanometer-sized particles that have found numerous applications[4] such as in cancer detection via biofunctionalization of the particles for immunoassay of the associated biomarker.[5] Various methods to synthesize silica nanoparticles have emerged[6,7] including a bioleaching process using sand.[8] Recent nanoindentation measurements have provided an elastic modulus of around 70 GPa for individual silica nanoparticles.[9] Carbon, on the other hand, is a major constituent of a cell of living organisms. Very recently, using scanning near field ultrasonic holography (SNFUH)[3] we reported that single-walled carbon nanohorns[10] could be visualized within mouse broncheoalveolar macrophages following particle delivery by aspiration.[11] However, phase localization of noncarbonaceous particles (with stiffness and density different than those of the nanohorns) has not been fully explored despite the highly debated dependence of nanoparticle chemical composition and size in cellular entry.[1,2] Here, using synthesized silica nanoparticles, initially in colloidal form and with diameters of about 87 nm,[12] we first investigate the probe-sample coupling that leads to the formation of the phase image and show that compositionally different stiff nanoparticles can be, with nanometer resolution, locally characterized within a macrophage. The measured diameters of the detected particles agree well with reported scanning electron microscope (SEM) images and optical spectra.[12,13]

The result of the chemical preparation of the samples is the silica-exposed cells immobilized on a mica substrate [Fig. 2(a)]. Ultrasonic energy at a frequency of 3.950 MHz is coupled into the cells (typically 25 μm in diameter) via a piezoelectric crystal below the mica. If a SiO_2 nanoparticle has been embedded within the cell, then it may induce sufficient scattering. Operating an atomic force microscope (AFM) in the contact mode, an instance of subsurface localization was implemented by oscillating the microcantilever of the AFM at 4.217 MHz. Using a lock-in amplifier, the onset of a coupling between the oscillations of the cell and the cantilever was established by detecting a phase signal at a frequency of $|f_c - f_s|$. Figure 1(a) depicts the approach of the cantilever to the sample [Fig. 1(a) (left)], where no measurable coupling is observed [Fig. 1(c) (left)]. The occurrence of the coupling to the sample surface is shown in Fig. 1(a) (right) [schematically depicted in Fig. 1(b) (right)] corresponding to the emergence of the peak in Fig. 1(c) (right). We note that in all results, the signals measured originate from a monitoring of the cantilever dynamics alone. We note that the strength of the coupling, that is, the emergence of the peak at $|f_c - f_s|$, is also a function of the driving amplitudes of both piezoelectric crystals (in our case, the amplitude used was 2 $V_{p.p.}$ for both), as well as a function of the different frequency pairs (f_s, f_c), albeit the value of the individual fre-

a)Electronic mail: passianan@ornl.gov.

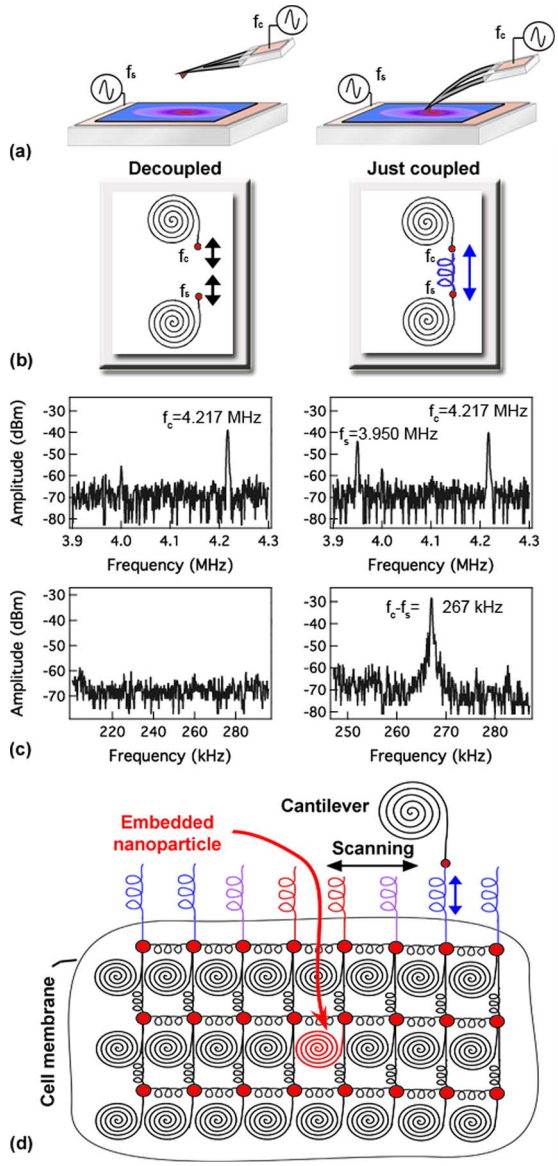

FIG. 1. (Color online) The mechanism of the nonlinear coupling and the emergence of the corresponding spectral peak. (a) Representation of the coupling (right column) and decoupling (left column) between the microcantilever and the sample, (b) their equivalent oscillator model, and (c) measured frequency spectra. (d) Pictorial anatomy of the cantilever-nanoparticle-cell system under SNFUH.

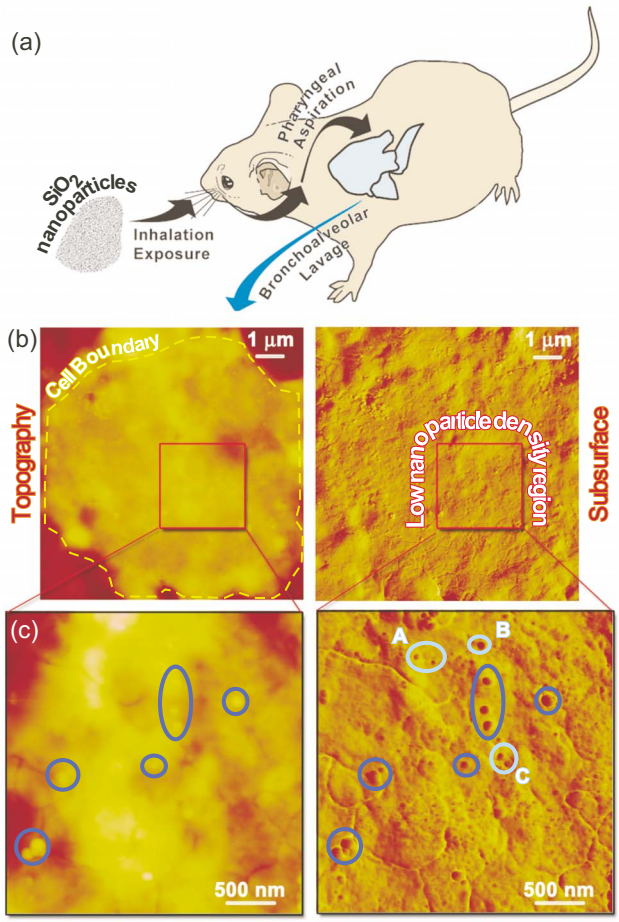

FIG. 2. (Color online) Topographic and subsurface localizations of nanoparticles in alveolar macrophages from SiO_2-exposed mice. The exposure route and cell sample origin are illustrated in (a). AFM topography [(b) and (c) (left)] and SNFUH phase [(b) and (c) (right)] images from a cell extracted 24 h after exposure. A selected region in (b) is rescanned at higher resolution and shown in (c), where ovals indicate the presence of silica. The dark blue ovals contain SiO_2 that reside on or just below the cell membrane while A, B, and C show nanoparticles deep within the cell.

quencies is less crucial than the difference in frequencies. In the simplest scenario [see Figs. 1(a) and 1(b)], one may pictorially consider a dynamic system where two independent slightly damped harmonic oscillators may approach each other such that, within some separation, a distance dependent coupling occurs (as a result of the interaction forces at the interface such as the repulsive forces of the contact mode AFM). Representing the oscillators with point masses attached to springs, the coupling may similarly be represented with yet another spring (neglecting surface damping). In analogy with phonon propagation in the bulk as well as in the surface region of solids, picturing the entire cell as being composed of interconnected oscillators such that the embedded nanostructure can be presented as an oscillator with a different set of elastic parameters, one may explain the acquired signal by SNFUH as a variation in the phase amplitude at the surface. A mechanical representation of the experimental system is illustrated in Fig. 1(d), where the buried nanoparticle has been represented as a different bulk oscillator (shown in red), and the probe has been implicated as interacting with the surface atoms of the sample via a different oscillator (blue). Additionally, the variation in the nanoparticle-induced phase perturbation has been pictured as a color gradient (blue to red).

Figure 2(a) illustrates the exposure route as well as the technique used to provide the samples. The results of cellular subsurface localization of the SiO_2 nanoparticles are shown in Figs. 2(b) and 2(c). The average diameter of the particles was measured to be 95 nm. In the topographic image of an alveolar macrophage from an exposed mouse, shown in Fig. 2(b) (left), the cell boundary has been marked by a yellow dashed line. The corresponding SNFUH phase image, shown in Fig. 2(b) (right), remarkably reproduces the overall subsurface landscape of the cell. Targeting a low nanoparticle number density region [as indicated in Fig. 2(b)], high resolution topographic and phase images consistently resolve individual nanoparticles. While Fig. 2(b) (left) and Fig. 2(c) (left) show nanoparticles on or just below the surface of the cell [circled in purple in Fig. 2(c)], Fig. 2(b) (right) and Fig. 2(c) (right) also transpire those contained within the cell [circled in blue in Fig. 2(c) and labeled A, B, and C]. Thus

the topographic features [demarcated with blue ovals in Fig. 2(c) (left) with varying contrast] within the resolution of the contact mode AFM appear to be surface bound. Intracellular particles sufficiently near the membrane (so as to modify the local curvature of the membrane) may be observed in this mode. We have observed such near surface distributions with both silica nanoparticles and agglomerated carbon nanohorns. Particles demarcated with light blue ovals [labeled with A, B, and C in Fig. 2(c) (right)] are buried silica deeper within the cellular structure (a cell thickness of 1 μm was typically measured in our work). Currently, lack of quantitative depth perception/resolution of the subsurface imaging techniques limits the measurements to qualitative assessment of the subsurface population only. In Fig. 2(c) (right), we show the detected silica (with an average diameter of 95 nm) within the cell, which are absent in the topography image in Fig. 2(c) (left): the height scale ranges in 0–80 nm for this section of the topography, excluding that a 90 nm diameter particle could reside on the top surface of the cell (would have appeared on a line profile).

The subsurface images in Figs. 2(b) and 2(c) present a different contrast, which can be explained on the basis of the different parameters used in each case: in Fig. 2(b) the piezoelectric crystal of the sample was vibrated at a frequency of 3.955 MHz and an amplitude of 2.00 $V_{p.p.}$ while in Fig. 2(c) it was oscillated at a frequency of 3.970 MHz and an amplitude of 2.83 $V_{p.p.}$. Similarly the piezoelectric crystal located on the cantilever was vibrated at a frequency of 4.200 MHz and an amplitude of 1.70 $V_{p.p.}$, whereas in Fig. 2(c) it was oscillated with an amplitude of 1.60 $V_{p.p.}$.

We note that the low silica nanoparticle density (particles delivered via aspiration), the random nanoparticle distribution, the chemical composition/optical properties of the nanoparticles, and the large size of an individual cell are all of consequence to the measurements presented. For example, micro-Raman spectroscopy did not yield any significant information (searching for the Si–O–Si bands) due to low silica density from macrophages on a mica substrate (generally the silica used do not possess any pronounced Raman features). In this regard, the use of SNFUH appears to be most useful. For the same reasons, SEM and x-ray photoemission spectroscopy (XPS) (while verifying the composition of the substrate and the buffer) were attempted and proved less instrumental in providing further information. Similarly, the particles being generally amorphous and lacking strong crystalline structure, x-ray diffraction (XRD) is not anticipated to yield useful data on the macrophage-silica system.

Particle specific nanoscale properties such as the Young modulus and electronic and optical properties have not been consistently and adequately reported in the literature for the nanomaterials used. This lack of quantitative knowledge is expected to limit the kinds of comparisons that can be made from the images acquired. However, geometric factors such as nanoparticle size, shape, and density and distribution may lend themselves to comparisons.

In conclusion, we have demonstrated that embedded stiff nanomaterials such as SiO_2 in a cell can be visualized with high resolution using SNFUH. Noting that, while using force curve measurements, we verified that the local adhesive and elastic properties shift when the cantilever approaches the cell surface, the surface of the silica nanoparticle on the cell surface, or the mica substrate; no subsurface information could be achieved without explicitly employing the nonlinear coupling of the cantilever to the sample, and thus, it can be concluded that the utility of SNFUH for mapping stiff nanoparticles within biological samples is indispensable. Therefore, the presented results will be important in nanomaterial design and characterization for biological applications. The transport, physical and chemical attachments, and embedding of nanomaterials within cells, as well as eventual cellular configurational changes, can therefore be studied noninvasively.

This research was sponsored by DOE-OBER. We are indebted to W. Wang and B. Gu of ORNL for their support and for supplying silica, and D. Glass for help with animal experiments. Research of V.P.D. and G.S. was supported by NSF-NSEC and SRC. We are grateful to V. Castranova at NIOSH for training with the pharyngeal aspiration and BAL techniques. ORNL is managed by UT-Battelle, LLC, for the U.S. Department of Energy under Contract No. DE-AC05-00OR22725.

[1] T. Xia, L. Rome, and A. Nel, Nature Mater. **7**, 519 (2008).
[2] A. Verma, O. Uzun, Y. Hu, Y. Hu, H.-S. Han, N. Watson, S. Chen, D. J. Irvine, and F. Stellacci, Nature Mater. **7**, 588 (2008).
[3] G. S. Shekhawat and V. P. Dravid, Science **310**, 89 (2005).
[4] W. Tan, K. Wang, X. He, X. J. Zhao, X. T. Drake, L. Wang, and R. P. Bagwe, Med. Res. Rev. **24**, 621 (2004).
[5] J. Wang, G. Liu, M. H. Engelhard, and Y. Lin, Anal. Chem. **78**, 6974 (2006).
[6] C.-H. Lu, W.-H. Zhou, B. Han, H.-H. Yang, X. Chen, and X.-R. Wang, Anal. Chem. **79**, 5457 (2007).
[7] J.-F. Chen, H.-M. Ding, J.-X. Wang, and L. Shao, Biomaterials **25**, 723 (2004).
[8] V. Bansal, A. Sanyal, D. Rautaray, A. Ahmad, and M. Sastry, Adv. Mater. (Weinheim, Ger.) **17**, 889 (2005).
[9] M. Zou and D. Yang, Tribol. Lett. **22**, 189 (2006).
[10] S. Iijima, M. Yudasaka, R. Yamada, S. Bandow, K. Suenaga, F. Kokai, and K. Takahashi, Chem. Phys. Lett. **309**, 165 (1999).
[11] L. Tetard, A. Passian, K. T. Venmar, R. M. Lynch, B. H. Voy, G. S. Shekhawat, V. P. Dravid, and T. Thundat, Nat. Nanotechnol. **3**, 501 (2008).
[12] W. Wang, B. Gu, L. Liang, and W. A. Hamilton, J. Phys. Chem. B **107**, 3400 (2003).
[13] W. Wang, B. Gu, L. Liang, and W. A. Hamilton, J. Phys. Chem. B **107**, 12113 (2003).